Journal of Applied Sciences

ISSN 1812-5654

science alert

ANSInet
an open access publisher
http://ansinet.com

Journal of Applied Sciences 10 (23): 3021-3031, 2010
ISSN 1812-5654

Satellite Retrieval of Aerosol Optical Thickness over Arid Region: Case Study over Makkah, Mina and Arafah, Saudi Arabia

N. Othman, M.Z. Mat Jafri, H.S. Lim and K. Abdullah
School of Physics, Universiti Sains Malaysia, 11800 Penang, Malaysia

Abstract: In this study, we presents the potentiality of retrieving Aerosol Optical Thickness (AOT) in the atmosphere which combined Landsat 7 ETM+ satellite and ground based closures enable the determination of required aerosol characteristics over moderate bright surfaces area of Makkah, Mina and Arafah. A multispectral algorithm was developed by assuming that surface condition of study area was lambertian and homogeneous. *In situ* AOT data was calculated using Beer Lambert law from transmittance of atmospheric measured using the FieldSpec handheld spectroradiometer and their locations were determined by a handheld Global Positioning System (GPS). The Digital Number (DN) recorded by satellite imageries were converted to top of the atmosphere (TOA) reflectance which is the sum of the ground reflectance and atmospheric reflectance. Then, the atmospheric correction (ATCOR2) method was used to retrieve the surface reflectance. The reflectance measured from the satellite at the top of the atmosphere (TOA) was subtracted from the amount given by the surface reflectance to obtain the atmospheric reflectance. Measured PM10 and AOT were correlated with atmospheric reflectance value using regression technique. Various types of regression algorithms were then examined by comparing the correlation coefficient (R) values and the Root-Mean-Square Error (RMSE) values. The three band model of algorithm was selected based on the highest R value and the lowest RMSE value. The proposed algorithm added evidence on the correlation found between aerosol optical thickness derived from Landsat 7 ETM+ satellite using multispectral algorithm with Terra Multiangle Imaging SpectroRadiometer (MISR) AOT product.

Key words: Spectroradiometer, atmospheric reflectance, ATCOR2, TOA, multispectral algorithm

INTRODUCTION

Satellite remote sensing has provided quantitative information on aerosols with accuracy comparable to that of surface measurements. The use of earth observation to assess and map the atmospheric pollution in different geographical areas and especially in cities has received considerable attention from researchers who developed a variety of techniques (Kaufman *et al*., 1990; Sifakis and Deschamps, 1992; Retalis *et al*., 1999; Wald and Baleynaud, 1999; Wald *et al*., 1999; Hadjimitsis, 2009). The key parameter for assessing atmospheric pollution in photochemical air pollution studies is the aerosol optical thickness (Kaufman *et al*., 1990), which is also the most important unknown parameter in every atmospheric correction algorithm for solving the Radiative Transfer (RT) equation and removing atmospheric effects from satellite remotely sensed images (Kaufman and Tanre, 1996; Kaufman and Sendra, 1988; Hadjimitsis and Clayton, 2008). Single scattering approximation was used in this study related to aerosol scattering.

The large-scale distribution of aerosol concentration and characteristics, aerosol radiative forcing and property changes of clouds interacting with aerosols are among the important observations that can be provided by satellite remote sensing (Xingna *et al*., 2009). Due to the growing recognition of the importance of aerosol properties for studies of climate and global change, it is indeed fortunate that a number of very significant and greatly enhanced satellite systems are being developed for launch in the next few years. Satellite measurements can also be inverted to yield information on Aerosol Optical Thickness (AOT), angular scattering properties and size distribution (Lee *et al*., 2008). Satellite measurements clearly have the advantage of being the only set of measurements that provide a wide coverage.

The optical characteristics of atmospheric aerosol are needed in order to derive the AOT and mass burden from path radiance measurements taken from space (Fraser *et al*., 1984; Kaufman and Sendra, 1988; Holben *et al*., 1992; Martonchik and Diner, 1992), or the aerosol single-scattering albedo (Kaufman, 1987) and the

Corresponding Author: N. Othman, School of Physics, Universiti Sains Malaysia, 11800 Penang, Malaysia
Tel: +604-6533888 Fax: +604-6579150

particle size (Kaufman *et al*., 1990). Satellite data are well suited to study aerosol effects on the large scale of area (Kaufman *et al*., 2002). The first applications of satellite remote sensing of aerosols began in the mid-1970s and concerned the detection of desert particles above the ocean (Fraser, 1976; Norton *et al*., 1980; Griggs, 1979). They used Land observing satellite (Landsat), Geostationary Operational Environmental Satellites (GOES) and Advanced Very High Resolution Radiometer (AVHRR) data, respectively. Crist *et al*. (1986) describe the method to normalize Landsat data affected by haze, using the third feature of the Tasseled Cap transformation. This study shows that atmospheric scattering decreases in severity with increasing the wavelength and since the visible bands of the Landsat Multispectral Scanner (MSS) sensor (i.e., band 1 and 2) are highly correlated in their response to surface features, a contrast of these two bands, as represented in yellowness, could be expected to provide atmospheric scattering information.

There are two major sources of aerosol data: (1) satellite instruments, such as AVHRR-2, Global Ozone Monitoring Experiment (GOME), Total Ozone Mapping Spectrometer (TOMS), Sea-viewing Wide Field-of-view Sensor (SeaWiFS), POLarization and Directionality of the Earth's Reflectances (POLDER), Moderate Resolution Imaging Spectroradiometer (MODIS) and Multiangle Imaging SpectroRadiometer (MISR) and (2) ground-based instruments, such as a narrow band sun photometer (Schaap *et al*., 2008) and spectroradiometer (Brogniez *et al*., 2008). Both these equipments can be correlated with the satellite sensor's electromagnetic spectrums. Therefore, these equipments are able to collect values of the AOT in the same wavelength bands of the satellite imagery. Those permanent narrow band sun photometer and spectroradiometer used widely is AErosol RObotic NETwork (AERONET) (Holben *et al*., 1998) and RSS-1024 Rotating Shadowband Spectroradiometer (Harrison *et al*., 1999), respectively. These equipments also come in handy as it is mobile and able to collect the optical readings anywhere such as MICROTOPS II hand-held sunphotometer and FieldSpec handheld spectroradiometer (Lim *et al*., 2009).

This study presents a new method of assessing atmospheric pollution in arid regions using satellite remote sensing technology. The method involves the use of beer lambert law for determining the aerosol optical thickness from handheld spectroradiometer data. Therefore the use of aerosol optical thickness was found in the literature to be a valuable parameter to assess air pollution (Sifakis and Descamps, 1992; Retalis, 1998). The determined aerosol optical thickness is therefore with various type of multispectral algorithm used for assessing atmospheric pollution from satellite imagery. The proposed method was initially applied to two Landsat 7 ETM+ images over Makkah, Mina and Arafah. Then, the results were compared with Terra MISR AOT product.

MATERIALS AND METHODS

Study area: Figure 1 shows the selected study area of Makkah, Mina and Arafah over Saudi Arabia. The Holy City of Makkah was an arid-urban area (Latitude 21°25'19" North Meridian 39°49'46") is at an elevation of 277 m above sea level and approximately 80 km inland from the Red Sea. The elevations of Makkah AI Mukarramah are a group of mountains and black rocky masses which are granitic basement rocks (Al-Jeelani, 2009). Mountains are traversed by a group of valleys, such as the Ibrahim valley. The Kaabah's location is in this valley.

Saudi Arabia is located in a dry area where precipitation rarely occurs and surface winds are inactive almost all the year round. In Saudi Arabia, dust plays a primary role in causing air pollution in a country which is than 90% desert. The desert is the source region of dust (PME, 2007). The desert is characterized by periodical outbreaks of dust storms that transport large amounts of desert dust in the troposphere, resulting in enhanced of optical thickness value that is correlated with the aerosol direct radiative forcing. Increase in the number of pilgrim's is accompanied by the increase of their daily activities as well as the increase of the demands of transportation means. Consequently, considerable quantities of either gaseous or solid pollutants are emitted to the atmosphere. The emitted pollutants could cause many harmful environmental impacts to the Holy City of Makkah and nearby places. Some studies about air pollution that had been carried out in the Holy City of Makkah, Saudi Arabia, focusing on the central area near the Holy Mosque and on the Holy places (Mina and Arafah) (Al-Jeelani, 2009; Al-Jeelani and Ramadhan, 2004).

Makkah climate is different from other Saudi Arabian cities, retains its warm temperature in winter (November to March), which can range from 17°C at midnight to 25°C in the afternoon. During summer (April to October), temperatures are considered very hot and break the 40°C mark in the afternoon dropping to 30°C in the evening. Rain is very rare with an average of 10-33 mm usually falls in December and January and the humidity ratio is about 45-53%. Winds are north-eastern most of the year time. Some unusual events often happen during the year, such as dust storms in summer, coming from the Arabian Peninsula's deserts or from North Africa (Al-Jeelani, 2009).

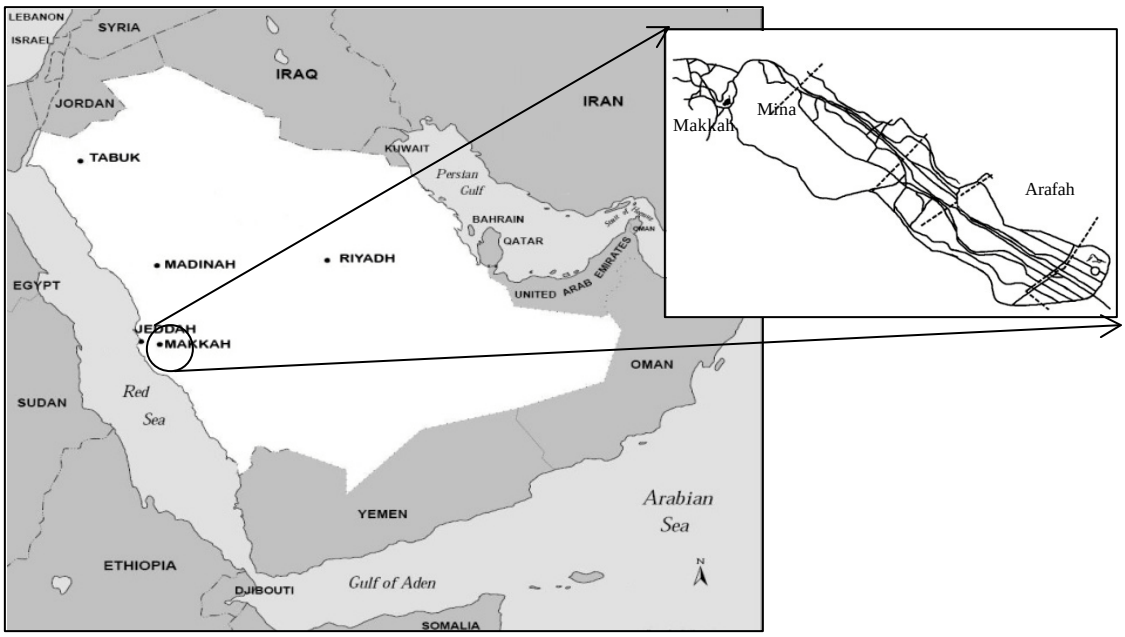

Fig. 1: Location of Makkah, Mina and Arafah

Table 1: Satellite imagery information

No.	Date	Description	Earth-Sun distance (d)	Visibility (km)	Sun angle (°)		
					Azimuth	Elevation	Zenith
1	29th December 2006	Hajj	0.9834	10	148.3622	38.1156	51.8844
2	19th January 2009	Non- Hajj	0.9839	10	144.0734	39.4352	50.5648

The methodology process generally were divided into four major parts: data acquisition, pre-processing, data processing and finally, accuracy and validation of results. All data preprocessing and processing steps were carried out using PCI Geomatica 10.2 software.

Data acquisition

Satellite image: The Earth observing instrument on Landsat 7 ETM+, the Enhanced Thematic Mapper Plus (ETM+), replicates the capabilities of the highly successful Thematic Mapper instruments on Landsats 4 and 5 TM. On May 31, 2003, the Scan Line Corrector (SLC), which compensates for the forward motion of Landsat 7 ETM+, failed. The Landsat 7 ETM+ continues to acquire image data in the SLC-off mode with the same high radiometric and geometric quality as that of the data collected prior to the SLC failure. The malfunction of the SLC mirror assembly resulted in the loss of approximately 22% of the normal scene area (Storey *et al*., 2005). Note that the SLC failure has no impact on the radiometric performance with the valid pixels. All scenes were affected by the failure in SLC (SLC-off mode) that occurred after 2003, so parts of the data in the scenes are lost.

The acquisition dates of the Landsat ETM+ scenes employed in the air quality change detection process within seasonal variation (Hajj season and non-Hajj season) were captured at WRS Path/Row 169/45 on 29th December 2006 and 19th January 2009, respectively. All Landsat 7 ETM+ scenes were downloaded from the United States Geological Survey (USGS) as a Level 8 product based on the minimum percentage of cloud cover (<10%) and the availability of ground truth data prior to acquisition. These imageries were acquired in NLAPS format 30×30 m pixels.

To reduce effect due to zenith angle and surface reflectivity effect, both imageries were selected among the same value for sun zenith angle, azimuth angle. The images and acquisition of Landsat 7 ETM+ scenes analyzed in this study are listed in Table 1.

Ground truth data: The ground truth data were obtained from the field survey covers all type of ground surface and scattered point throughout Makkah, Mina and Arafah using FieldSpec handheld spectroradiometer. FieldSpec handheld spectroradiometer was used to measure the transmittance values at the ground surface. Atmospheric transmittance at wavelength, T_λ may be computed as Jensen (1995):

$$T_\lambda = \frac{I_\lambda}{I_{o\lambda}} = \exp(-\tau_\lambda M) \quad (1)$$

Where:

I_λ = The solar irradiance reached the ground at wavelength (λ)

$I_{o\lambda}$ = Solar irradiance at the top of atmosphere at wavelength (λ)

τ_λ = Total atmospheric optical thickness at wavelength (λ)

M = Relative optical mass. M = 1 when the sun is directly overhead and is otherwise approximately equal to sec (z), where z is the solar zenith angle

According to the Bouguer-Lambert law, also known as Beer's law (Mather, 2004), the attenuation of light through a medium is proportional to the distance traversed in the medium and the local flux of radiation. The positions of each station were determined using GPS equipment. All ground data were taken less than 3 h within 9.00 a.m. to 12.00 p.m. to reduce the uncertainty due to wind and solar zenith angle. The measurements time was corresponding to the time of Landsat 7 ETM+ and Terra which overpass at 10.15 a.m. and 10:30 a.m. equator crossing time, respectively (Williams, 2009). The ground truth data of AOT were divided into two groups; half of the numbers were randomly selected for calibration of algorithm and the other half for accuracy analysis. Presumption made in this study was that each AOT measurement represents a locus of 1 pixel of Landsat 7 ETM+ data equal to 30×30 m at ground around each of the air pollution stations.

Pre-processing

Geometric and distortion correction: The Landsat 7 ETM+ satellite image was rectified using the second order polynomial coordinates transformation to relate groud control points in the map to their equivalent row and column positions in the Landsat 7 ETM+ scences. Corrected images were projected to Universal Transverse Mercator Projection with UTM 37 Q D000 WGS 1984 Datum. The reference points used to resample the satellite images were taken from 14 Ground Control Point (GCP) collected at study area.

Radiometric and atmospheric correction: Typically, the user of the data can convert the received DN values into radiances by simple linear formulas using calibration gains and offset. Radiometric correction is applied by transforming the values of DN to radiance or reflectance values through the algorithm as follows given by Chander *et al*. (2009):

Table 2: Gain and offset value for Landsat 7 ETM+

No.	c0	c1 (mW/cm^2/sr/μm)
1	-0.7380	0.1180709
2	-0.7610	0.1209843
3	-0.5940	0.0942520
4	-0.5740	0.0639764
5	-0.1190	0.0191220
6	-0.0070	0.0067087
7	-0.0420	0.0066496

$$L_\lambda = (\text{Grescale}) \times (\text{QCAL} + \text{Brescale}) \quad (2)$$

The value of Grescale (c1) and Brescale (c0) for Landsat 7 ETM+ used in this study can be found in Table 2. Also can be expressed as:

$$L_\lambda = \left(\frac{\text{LMAX}_\lambda - \text{LMIN}_\lambda}{\text{QCALMAX} - \text{QCALMIN}}\right) \times (\text{QCAL} - \text{QCALMIN}) + \text{LMIN}_\lambda \quad (3)$$

Where:

L_λ = Spectral Radiance at the sensor's aperture in W/m^2/sr/μm

Grescale = Rescaled gain (the data product gain contained in the Level 1 product header or ancillary data record) in W/m^2/sr/μm/DN

Brescale = Rescaled bias (the data product offset contained in the Level 1 product header or ancillary data record) in W/m^2/sr/μm

QCAL = The quantized calibrated pixel value in DN

LMIN_λ = The spectral radiance that is scaled to QCALMIN in W/m^2/sr/μm

LMAX_λ = The spectral radiance that is scaled to QCALMAX in W/m^2/sr/μm

QCALMIN = The minimum quantized calibrated pixel value (corresponding to LMIN_λ) in DN

For relatively clear Landsat scenes, a reduction in between-scene variability can be achieved through a normalization for solar irradiance by converting spectral radiance, as calculated above, to planetary reflectance or albedo. This combined surface and atmospheric reflectance of the Earth also known as top of atmosphere reflectance (TOA) is computed with the following formula (Mather, 2004):

$$\rho_p = \frac{\pi L_\lambda d^2}{\text{ESUN}_\lambda \cos\theta_S} \quad (4)$$

Where:

ρ_p = Unitless planetary reflectance

L_λ = Spectral radiance at the sensor's aperture

d = Earth-Sun distance in astronomical units (Table 1, Chander *et al*., 2009)

Table 3: ETM+ solar spectral irradiances (generated using the Thuillier solar spectrum)

Band	W/m²/μm
1	1997.00
2	1812.00
3	1533.00
4	1039.00
5	230.80
6	84.90
7	1362.00

$ESUN_\lambda$ = Mean solar exo-atmospheric irradiances (Table 3, Chander *et al*., 2009)

θ_s = Solar zenith angle in degrees (Meta data of Landsat 7 ETM+)

Atmospheric correction was carried out using ATCOR2 available with PCI Geomatica using algorithms developed by Richter (1996a, b, 1997, 2005) and Richter *et al*. (2009). It calculates correction for flat areas applying constant or varying atmosphere accounting for adjacency effect. Atmospheric corrections widely used in hyper spectral imagery to derive surface reflectance without atmospheric effects.

Automatic calculate haze and cloud' would be the first run of ATCOR. The output files containing the haze and cloud mask. This mask can be edited if haze is not correctly assigned, e.g. defining additional haze areas or deleting wrongly assigned haze areas (Wen and Yang, 2008). Then ATCOR could be run again with Load Haze and cloud from file employing this edited mask, which might yield better results for the haze removal.

The atmospheric correction algorithm calculates the surface reflectance using the default scale factor 4, i.e., the percent reflectance range 0-100% is multiplied with the factor 4 in the output file. So an output value of DN = 200 corresponds to a surface reflectance of 200/4 = 50% (or 0.5 for 0-1 reflectance range) and the output is coded as 8 bit/pixel. Therefore, the maximum output value is 255, representing a surface reflectance of 255/4 = 63.75% (PCI Geomatics Enterprises Inc., 2005). Larger values will be truncated at 255. ATCOR2 is based on a database of atmospheric correction functions stored in look-up tables. The database consists of a broad range of elevation information setup, sensor information, atmospheric information and correction parameter as in Table 4. All meteorological data used in this study were taken from Weather Underground (2009) webpage. Cogliani (2001) and Rodriguez *et al*. (2009) also used Weather Underground (2009) in their research. The result of ATCOR2 is a ground or surface reflectance image in each spectral band with a relative error of approximately 10% (Lehner *et al*., 2004).

Data processing: After undergo radiometric correction, the reflectance measured from the satellite (reflectance at the top of atmospheric, TOA) was subtracted by the amount given by the surface reflectance to obtain the atmospheric reflectance. The atmospheric reflectance satellite data were related with AOT in-situ data using the regression algorithm analysis. PCI Geomatica EASI modeling was used to input the developed multispectral algorithm. AOT maps were generated using proposed algorithm based on the highest R and lowest RMSE values. The final results were in color coded image of AOT.

Table 4: Input parameter for ATCOR2

Input parameter	Input value
Elevation information setup	
1. Height	0.240
2. Unit	km
Sensor information	
1. Sensor Type	Landsat 7 ETM+
2. Pixel size	30.00 m
3. Date	Table 1
4. Calibration file	Table 2
Atmospheric information	
1. Atmospheric definition area	Rural
2. Thermal atmospheric definition	Arid
3. Condition	Dry
Correction parameter	
1. Solar zenith	Table 1
2. Visibility	Table 1
3. Adjacency	1.0 km
4. Offset to surface temperature	0.0K

Algorithm model: The approach of this study begins with the assumption of a Lambertian surface in algorithm development, so that the surface reflective property will not be affected by the observation geometry or terrain effect. In reality, surface condition over study area is not Lambertian, which implies that the results of the retrieved AOT would be influenced by the surface canopy, observation geometry or terrain effects. The Mie (aerosol) scattering theory was applied to compute the aerosol phase function and spectral optical depth, based on size distribution, real and imaginary index (King *et al*., 1999; Fukushima *et al*., 2000).

$$\rho_a(\theta_s, \theta_v, \phi) \approx \frac{\omega_o \tau_a P_a(\theta_s, \theta_v, \phi)}{4\mu\mu_o} \quad (5)$$

Where:

ρ_{atm} = Atmospheric reflectance/path radiance

ρ_a = Path radiance due to aerosol scattering

P_a = Aerosol scattering phase function

θ_s = Solar zenith angle

θ_v = Viewing zenith angle

ϕ = Relative azimuthal angles

ω_o = Single scattering albedo

μ = Cosines of the view directions

μ_o = Cosines of the illumination directions

Semi-infinite cloud was now abandoned and turn to the more realistic case of cloud layer with finite optical depth, τ. Then, that case is initially consider where scattering is conservative; i.e., $\omega_o \approx 1$. This assumption sounds drastic, but in fact the single scatter albedo of cloud droplets is very close to one over most of the visible band and absorption by clouds is indeed negligible for most purposes within that band. By neglecting molecule scattering due to Rayleigh (Paronis and Hatzopoulos, 1997), Eq. 5 becomes:

$$\tau_a = \left(\frac{4\mu\mu_o}{\omega_o P_a(\theta_s, \theta_v, \phi)}\right)\rho_{atm}(\theta_s, \theta_v, \phi) \quad (6)$$

Where:
AOT = τ_a
R = $\rho_a(\theta_s, \theta_v, \phi)$

$$a_o = \left(\frac{4\mu\mu_o}{\omega_o P_a(\theta_s, \theta_v, \phi)}\right)$$

So, the algorithm of AOT for single band or wavelength (λ) is simplified as:

$$AOT(\lambda) = a_o R(\lambda) \quad (7)$$

Equation 7 is rewrite into two and three band equation as Eq. 8 and 9:

$$AOT(\lambda) = a_o R_{\lambda 1} + a_1 R_{\lambda 2} \quad (8)$$

$$AOT(\lambda) = a_o R_{\lambda 1} + a_1 R_{\lambda 2} + a_2 R_{\lambda 3} \quad (9)$$

where, $R_{\lambda i}$ is the atmospheric reflectance (i = 1, 2 and 3 corresponding to wavelength for satellite) and a_j is the algorithm coefficient (j = 0, 1 and 2) are empirically determined.

Accuracy and validation of results: The accuracy assessment and validation of results obtained was performing with ground truth and other satellite product data. Accuracy and validation analysis of results were perform using the new algorithm with AOT ground truth values retrieved using handheld spectroradiometer. The AOT maps generated using developed algorithm also compared with aerosol product of AOT using Terra MISR MIL3DAElarc.004 level 3 component global aerosol product covering daily statistical summary 0.5×0.5 degree aerosol product over selected individual locations which is Makkah, Mina and Arafah with respect to the Landsat 7 ETM+ subset for that particular day. The AOT are retrieved from the Terra MISR daytime data at wavelength 555 nm. Knowing that MISR satellite data has been well calibrated using ground truth data of AERONET (Lyapustin *et al*., 2007). The validation is reasonable because the different time between Landsat 7 ETM and Terra is about ±30 min, the Landsat 7 ETM+ equatorial crossing time from north to south on a descending orbital node between 10:00 a.m. to 10:15 a.m. on each pass Williams (2009) while, Terra MISR daily visit in sun-synchronous polar orbit with an equator crossing time of 10:30 a.m. (Diner *et al*., 1998, 2002).

RESULTS

Image analysis: A total of two dataset had been used for the development of multispectral algorithm in this study. The AOT values measured using FieldSpec handheld spectroradiometer from the ground truth data were correlated with atmospheric reflectance from Landsat 7 ETM+ in red, green and blue band. Distribution of AOT with respect to reflectance of atmosphere for red band ($R_{\lambda 3}$), green band ($R_{\lambda 2}$) and blue band ($R_{\lambda 1}$) shows as in Fig. 2, for combination dataset of 29th December 2006 and 19th January 2009. In this study, we used the regression equation to correlate the AOT measured by FieldSpec handheld spectroradiometer were correlated with Landsat 7 ETM+ red band ($R_{\lambda 3}$), green band ($R_{\lambda 2}$) and blue band ($R_{\lambda 1}$).

Table 5 shows the comparison value for R and RMSE values for various type of algorithm using regression analysis for combination dataset on 29th December 2006 and 19th January 2009. Thus, when applying the algorithm to the entire of Landsat 7 ETM+ image, the proposed regression algorithm as stated in Table 5 was used based on the highest R and lowest RMSE value. A

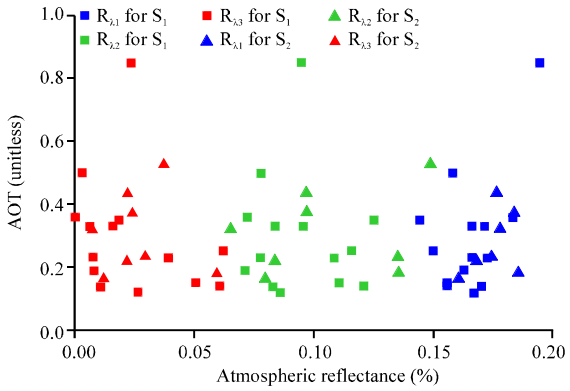

Fig. 2: Graph of AOT data versus atmospheric reflectance for three bands, $R_{\lambda 1}$, $R_{\lambda 2}$ and $R_{\lambda 3}$ for blue, green and red band, respectively on 29th December 2006 (S_1) and 19th January 2009 (S_2)

Table 5: Table of regression algorithm of PM10 combined datasets on 26th December 2006 and 19th January 2009

No.	Algorithm	R	RMSE	Coefficient
1	$a_0R_{\lambda1}+a_1R_{\lambda2}$	0.531	0.177	AOT = 2.80 $R_{\lambda1}$ - 1.81 $R_{\lambda2}$
2	$a_0R_{\lambda2}+a_1R_{\lambda3}$	0.255	0.202	AOT = 4.18 $R_{\lambda2}$ - 3.02 $R_{\lambda3}$
3	$a_0R_{\lambda1}+a_1R_{\lambda3}$	0.571	0.171	AOT = 1.91 $R_{\lambda1}$ - 0.46 $R_{\lambda3}$
4	$a_0R_{\lambda1}^2+a_1R_{\lambda2}^2$	0.559	0.173	AOT = 13.0 $R_{\lambda1}^2$ - 6.49 $R_{\lambda2}^2$
5	$a_0R_{\lambda1}^2+a_1R_{\lambda3}^2$	0.662	0.157	AOT = 10.9 $R_{\lambda1}^2$ + 4.1 $R_{\lambda3}^2$
6	$a_0R_{\lambda1}^3+a_1R_{\lambda2}^3$	0.594	0.168	AOT = 69.7 $R_{\lambda1}^3$ - 19.1 $R_{\lambda2}^3$
7	$a_0R_{\lambda1}^3+a_1R_{\lambda3}^3$	0.689	0.151	AOT = 64.6 $R_{\lambda1}^3$ + 79.1 $R_{\lambda3}^3$
8	$a_0R_{\lambda1}+a_1R_{\lambda2}+a_2R_{\lambda3}$	0.804	0.130	AOT = 5.34 $R_{\lambda1}$ - 8.40 $R_{\lambda2}$ + 5.69 $R_{\lambda3}$ (Proposed algorithm)
9	$a_0R_{\lambda1}^2+a_1R_{\lambda2}^2+a_2R_{\lambda3}^2$	0.725	0.151	AOT = 16.6 $R_{\lambda1}^2$ - 24.5 $R_{\lambda2}^2$ + 29.2 $R_{\lambda3}^2$

$R_{\lambda1}$, $R_{\lambda2}$ and $R_{\lambda3}$ are the reflectance values for blue, green and red band, respectively

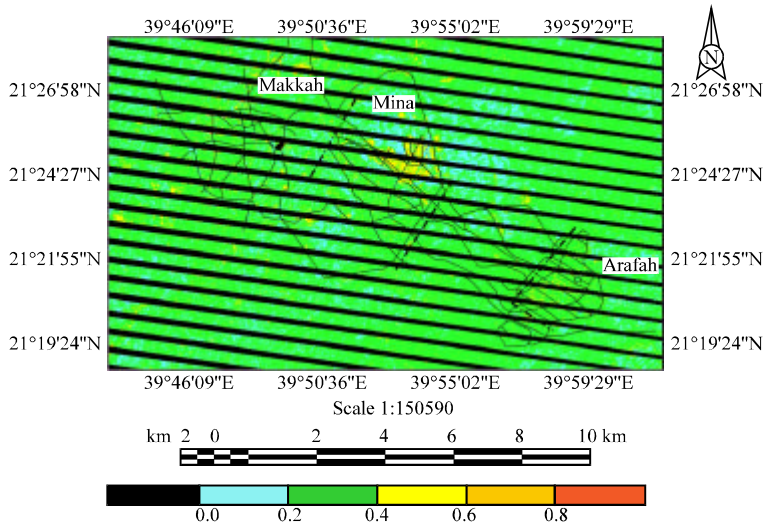

Fig. 3: AOT colour-coded maps on 29th December 2006

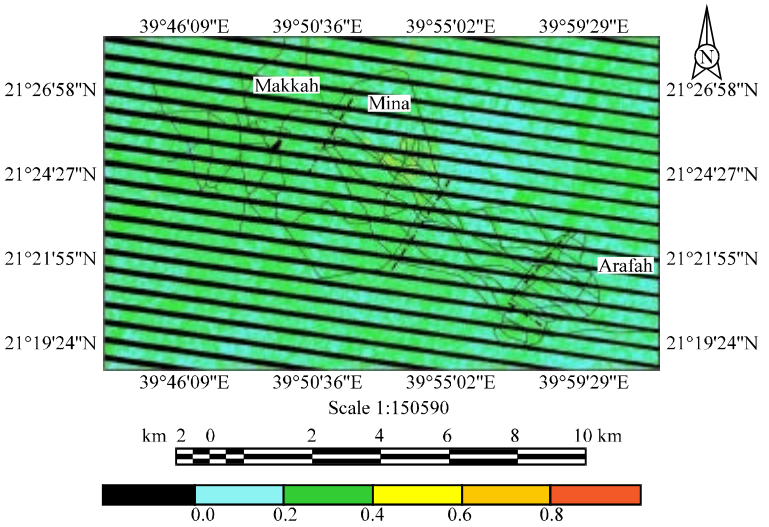

Fig. 4: AOT colour coded image on 19th January 2009

wide-coverage AOT map can be obtained conveniently. Figure 3 shows the distribution of AOT on 29th December 2006 which is Hajj season. Figure 4 is the distribution of AOT on 19th January 2009 which is non-Hajj season.

The AOT concentrations are indicated through the color of red for high AOT value and blue for low AOT value. The summarization the data percentage for each range of the AOT values by corresponding color coded

Table 6: Percentage of AOT color coded maps on 26th December 2006 and 19th January 2009

	Data percentage					
Date	Unfilled gap and cloud	0-0.2	0.2-0.4	0.4-0.6	0.6-0.8	0.8-1.0
29th December 2006	28.30	8.33	60.77	2.15	0.31	0.10
19th January 2009	32.63	31.09	35.22	0.50	0.23	0.30

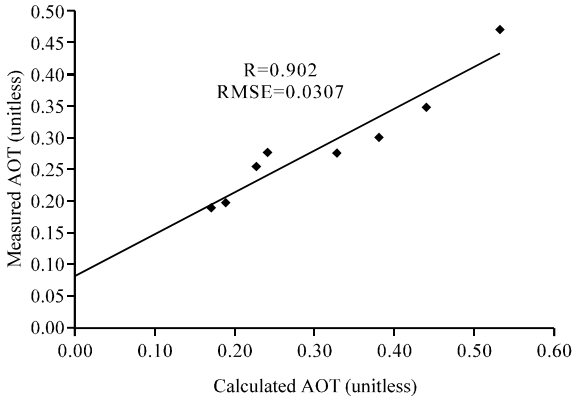

Fig. 5: Graph of measured AOT versus calculated AOT for 29th December 2006

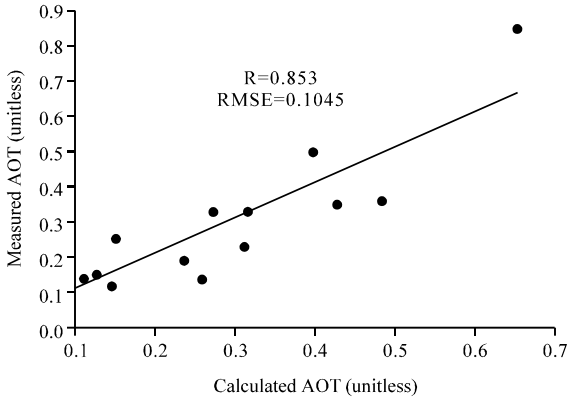

Fig. 6: Graph of measured AOT versus calculated AOT for 19th January 2009

classification for five days on 29th December 2006 and 19th January 2009 was presented in Table 6. It clearly showed the Hajj season is more polluted than non-Hajj season. The higher AOT distributed mainly at Makkah and Mina area where there was construction site generated a lot of dust and the values were relatively lower in rural area.

Validation of AOT algorithm

Ground truth data: Figure 5 shows the measured AOT and calculated AOT for 29th December 2006, where the measured AOT were the AOT measured using Fieldspec handheld spectroradiometer and calculated AOT were the AOT calculated using developed multispectral algorithm. Figure 6 shows measured AOT and calculated AOT

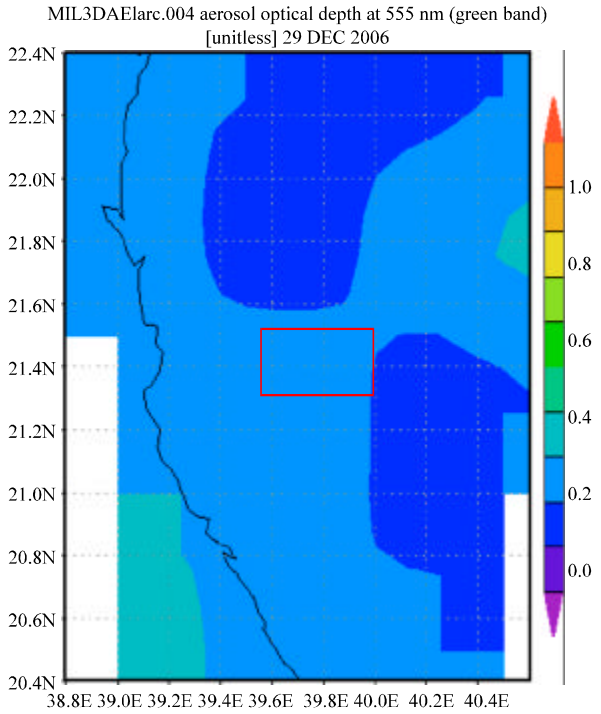

Fig. 7: Terra MISR AOT daily product at 555 nm on 29th December 2006

concentration for 19th January 2009. The validation of the results generated using multispectral algorithm of AOT shows that all dataset gives the accuracy >0.85 of R coefficient value and low RMSE. It clearly shows that the developed multispectral algorithm is worked excellently in determining AOT value within arid region of Makkah.

Satellite data-terra MISR: A close-up view of the typical temporal distribution of AOT can be compared with AOT distributions pattern mapped using multispectral algorithm retrieved using Landsat 7 ETM+ satellite images by examining the daily product AOT of Terra MISR over selected individual locations which is Makkah, Mina and Arafah as marked in red rectangular shape area with respect to the Landsat 7 ETM+ subset image. AOT concentrations are indicated through the color of red for high AOT value and blue for low AOT value. Figure 7 shows the image of Terra MISR AOT product where the subset of Landsat 7 ETM+ was located on 29th December 2006. Figure 8 shows the image of Terra MODIS AOT

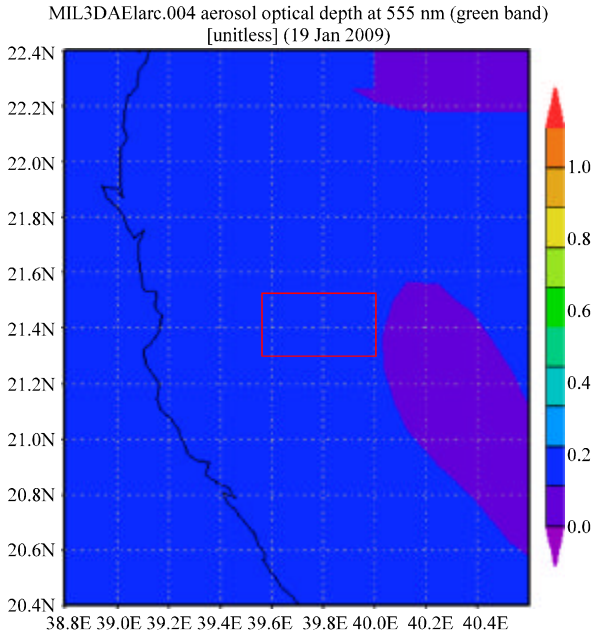

Fig. 8: Terra MISR AOT daily product at 555 nm on 19th January 2009

daily product on 19th January 2009. The resolution of MISR MIL3DAElarc.004 AOT is 0.5×0.5 degree.

DISCUSSION

High values of AOT were observed during Hajj season in 29th December 2006, while low values of AOT on 19th January 2009 is the consequence of non-Hajj season which reducing activities around study area. Physical geography and topography of the area corresponding to the surrounding area of rocky mountain known as valley area where enables a weak air flow contribute significantly to the high value of AOT around valley of Mina and Makkah. In addition, the construction activities were actively concentrated at Makkah and Mina produced a lot of dust pollution at nearby area. These variation could be attributed the metrological conditions, despite the little variation between the two successive years and Hajj circumstances. These studies showed that there were high concentrations of air pollutants in the atmosphere, exceeding the standards that are attributed to traffic emission during Hajj season, where about three million people gathered in these limited areas (Al-Jeelani and Ramadhan, 2004; Al-Jeelani, 2009). Also there was very high value of AOT near the Holy Mosque which showed the contribution of pollution by traffic and hajj pilgrimage (Al-Jeelani, 2009; Al-Raddadi, 1996). According to the results, both AOT data retrieved using multi temporal Landsat 7 ETM+ using the multispectral algorithm gives highly correlation with Terra MISR data at particular day. This is clearly seen where average AOT value retrieved using Landsat 7 ETM+ images located in the range of AOT product of Terra MISR value over Makkah, Mina and Arafah are low in non-Hajj season compared to Hajj season.

CONCLUSION

The number of ground stations present in urban air quality monitoring networks is usually not sufficient to produce reliable maps of particulate distribution over a considerable area. This study indicated that the feasibility of AOT retrieval technique by using a FieldSpec handheld spectroradiometer which shows that all dataset gives the accuracy >0.85 of R coefficient value. From the perspective of the AOT retrieved in this study, the AOT concentrations retrieved and mapped using developed multispectral algorithm in study area have correlation with data product form Terra MODIS and MISR at particular range. The Terra MISR is compatible to be used for the wide range of area with resolution of 0.5×0.5 degree aerosol product where Landsat 7 ETM+ has resolution of 30×30 m more suitable for small range of study area. The proposed technique can be used for the determination of the AOT values from the FieldSpec handheld spectroradiometer with a reasonable accuracy compared to Terra MISR data. The technique is a cheaper alternative to obtaining remotely sensed data for AOT studies.

ACKNOWLEDGMENTS

These researches were supported by USM-RU-PRGS PFIZIK/1001/831020 and FRGS (IPTA) 203/PFIZIK/6711107 (Hajj Research). Appreciations are extended to USM and all who involved in this research project. The images and data used in this study were acquired using the GES-DISC Interactive Online Visualization and analysis Infrastructure (Giovanni) as part of the NASA's Goddard Earth Sciences (GES) Data and Information Services Center (DISC).

REFERENCES

Al-Jeelani, H.A. and M.H. Ramadhan, 2004. Assessment of air quality in Mina and Makkah City during Hajj season. First year report submitted to the Institute of Research and Consultations, King Abdulaziz University.

Al-Jeelani, H.A., 2009. Evaluation of air quality in the Holy Makkah during Hajj season 1425 H. J. Applied Sci. Res., 5: 115-121.

Al-Raddadi, A.S., 1996. Study the air quality inside the souk alsagheer tunnel. First Report Submitted to Hajj Research Center, Aum Alqura University.

Brogniez, C., V. Buchard and F. Auriol, 2008. Validation of UV-visible aerosol optical thickness retrieved from spectroradiometer measurements. Atmospheric Chem. Phys., 8: 4655-4663.

Chander, G., B.L. Markham and D.L. Helder, 2009. Summary of current radiometric calibration coefficients for Landsat MSS, TM, ETM+ and EO-1 ALI sensors. Remote Sensing Environ., 113: 893-903.

Cogliani, E., 2001. Air pollution forecast in cities by an air pollution index highly correlated with meteorological variables. Atmospheric Environ., 35: 2871-2877.

Crist, E.P., R. Laurin and R.C. Cicone, 1986. Vegetation and soils information contained in transformed thematic mapper data. Proceedings of International Geoscience and Remote Sensing Symposium, (IGARSS'86), European Space Agency, Paris, pp: 1465-1470.

Diner, D.J., J.C. Beckert, T.H. Reilly, C.J. Bruegge and J.E. Conel *et al*., 1998. Multiangle imaging spectroradiometer (MISR) instrument description and experiment overview. Geosci. Remote Sens., 36: 1072-1087.

Diner, D.J., J.C. Beckert, G.W. Bothwell and J.I. Rodriguez, 2002. Performance of the MISR instrument during its first 20 months in Earth orbit. IEEE Trans. Geosci. Remote Sens., 40: 1449-1466.

Fraser, R.S., 1976. Satellite measurement of mass of Sahara dust in the atmosphere. Applied Optics, 15: 2471-2479.

Fraser, R.S., Y.J. Kaufman and R.L. Mahoney, 1984. Satellite measurements of aerosol mass and transport. Atmospheric Environ., 18: 2577-2584.

Fukushima, H., M. Toratani, S. Yamamiya and Y. Mitomi, 2000. Atmospheric correction algorithm for ADEOS/OCTS acean colar data: Performance comparison based on ship and buoy measurements. Adv. Space Res., 25: 1015-1024.

Griggs, M., 1979. Satellite observations of atmosphere aerosol during the EOMET cruise. J. Atmospheric Sci., 36: 695-698.

Hadjimitsis, D.G. and C.R.I. Clayton, 2008. The use of an improved atmospheric correction algorithm for removing atmospheric effects from remotely sensed images using an atmosphere-surface simulation and meteorological data. Meteorol. Appl., 15: 381-387.

Hadjimitsis, D.G., 2009. Aerosol Optical Thickness (AOT) retrieval over land using satellite image-based algorithm. Air Quality Atmosphere Health, 2: 89-97.

Harrison, L., M. Beauharnois, J. Berndt, P. Kiedron, J.J. Michalsky and Q. Min, 1999. The Rotating Shadowband Spectroradiometer (RSS) at SGP. Geophys. Res. Lett., 26: 1715-1718.

Holben, B.N., E. Vermote, Y.J. Kaufman, D. Tanre and V. Kalb, 1992. Aerosol retrieval over land from AVHRR data application for atmospheric correction. IEEE Trans. Geosci. Remote Sens., 30: 212-222.

Holben, B.N., T.F. Eck, I. Slutsker, T. Tanre and J.P. Buis *et al*., 1998. AERONET: A federated instrument network and data archive for aerosol characterization. Remote Sens. Environ., 37: 2403-2412.

Jensen, J.R., 1995. Introductory Digital Image Processing: A Remote Sensing Perspective. 2nd Edn., Prentice Hall, Upper Saddle River, New Jersy, ISBN: 0132058405, pp: 111-112.

Kaufman, Y.J., 1987. Satellite sensing of aerosol absorption. J. Geophys. Res., 92: 4307-4317.

Kaufman, Y.J. and C. Sendra, 1988. Algorithm for automatic atmospheric corrections to visible and near-IR satellite imagery. Int. J. Remote Sens., 9: 1357-1381.

Kaufman, Y.J., R.S. Fraser and R.A. Ferrare, 1990. Satellite measurements of large-scale air pollution: Methods. J. Geophys. Res., 95: 9895-9909.

Kaufman, Y.J. and D. Tanre, 1996. Direct and indirect methods for correcting the aerosol effect on remote sensing. Remote Sens. Environ., 55: 65-79.

Kaufman, Y.J., D. Tanre and O. Boucher, 2002. A satellite view of aerosols in the climate system. Nature, 419: 215-223.

King, M.D., Y.J. Kaufman, D. Tanre and T. Nakajima, 1999. Remote sensing of tropospheric aerosols from space: Past, present and future. Bull. Am. Meteorol. Soc., 80: 2229-2259.

Lee, K.H., D.H. Lee, Y.J. Kim and J. Kim, 2008. MODIS 500 $\times$ 500-m^2 resolution aerosol optical thickness retrieval and its application for air quality monitoring. Adv. Environ. Monitor., 10.1007/978-1-4020-6364-0_17

Lehner, S., I. Anders and G. Gayer, 2004. High resolution maps of suspended particulate matter concentration in the german bight. EARSeL eProc., 3: 118-126.

Lim, H.S., M.Z. MatJafri, K. Abdullah, C.J. Wong and M.N. Saleh, 2009. Aerosol optical thickness data retrieval over Penang Island, Malaysia. Proceedings of the Aerospace Conference, March 7-14, Big Sky, MT., pp: 1-6.

Lyapustin, A., Y. Wang, R. Kahn, J. Xiong and A. Ignatov *et al*., 2007. Analysis of MODIS-MISR calibration differences using surface albedo around AERONET sites and cloud reflectance. Remote Sens. Environ., 107: 12-21.

Martonchik, J.V. and D.J. Diner, 1992. Retrieval of aerosol optical properties from multi-angle satellite imagery. IEEE Trans. Geosci. Remote Sens., 30: 223-230.

Mather, P.M., 2004. Computer Processing of Remotely-Sensed Images. An Introduction. 3rd Edn., John Wiley and Sons, New York, pp: 111-119.

Norton, C.C., F.R. Mosher, B. Hinton, D.W. Martin, D. Santik and W. Kuhlow, 1980. A model for calculating desert aerosol turbidity over ocean from geostationary satellite data. J. Applied Meteorol., 19: 633-644.

PCI Geomatics Enterprises Inc., 2005. Geomatica® Focus. User Guide. Arcadia Publishing, Richmond Hill, Ontario, pp: 211.

PME, 2007. Sources of Pollution. PME., Saudi Arabia.

Paronis, D.K. and J.N. Hatzopoulos, 1997. Aerosol optical thickness and scattering phase function retrieval from solar radiances recorded over water: A revised approach. Proceedings of the IEEE International Geoscience and Remote Sensing Symposium, Aug. 3-8, Singapore, United States, pp: 1920-1922.

Retalis, A., 1998. Study of atmospheric pollution in large cities with the use of satellite observations: Development of an atmospheric correction algorithm applied to polluted urban areas. Ph.D. Thesis, Department of Applied Physics, University of Athens.

Retalis, A., C. Cartalis and E. Athanassiou, 1999. Assessment of the distribution of aerosols in the area of Athens with the use of landsat thematic mapper data. Int. J. Remote Sensing, 20: 939-945.

Richter, R., 1996a. A spatially adaptive fat atmospheric correction algorithm. Int. J. Remote Sensing, 17: 1201-1214.

Richter, R., 1996b. Atmospheric correction of satellite data with haze removal including a haze/clear transition region. Comput. Geosci., 22: 675-681.

Richter, R., 1997. Correction of atmospheric and topographic effects for high spatial resolution satellite imagery. Int. J. Remote Sensing, 18: 1099-1111.

Richter, R., 2005. Atmospheric/Topographic Correction for Satellite Imagery. Version 6.1, Remote Sensing Data Center, Wessling, Germany.

Richter, R., T. Kellenberger and H. Kaufmann, 2009. Comparison of topographic correction methods. Remote Sensing, 1: 184-196.

Rodriguez, R., A. Cortes and T. Margalef, 2009. Injecting dynamic real-time data into a DDDAS for forest fire behavior prediction. Proceedings of the 9th International Conference on Computational Science, May 25-27, Baton Rouge, LA, USA., pp: 489-499.

Schaap, M., R.M.A. Timmermans, R.B.A. Koelemeijer, G. de Leeuw and P.J.H. Builtjes, 2008. Evaluation of MODIS aerosol optical thickness over Europe using sun photometer observations. Atmospheric Environ., 42: 2187-2197.

Sifakis, N. and P.Y., Deschamps, 1992. Mapping of air pollution using SPOT satellite data. Photogrmmetric Eng. Remote Sensing, 58:: 1433-1437.

Storey, J.C., P. Scaramuzza and G. Schmidt, 2005. Landsat 7 scan line corrector-off gap filled product development. Proceedings of the 16th Conference on Global Priorities in Land Remote Sensing, (CPLRS'05), Sioux Falls, South Dakota, pp: 23-27.

Wald, L. and J.M., Balleynaud, 1999. Observing air quality over the city of Nantes by means of landsat thermal infrared data. Int. J. Remote Sensing, 20: 947-959.

Wald, L., L. Basly and J.M. Balleynaud, 1999. Satellite data for the air pollution mapping. Proceedings of the 18th EARseL Symposium on Operational Sensing for Sustainable Development, May 11-14, Enschede, The Netherlands, pp: 133-139.

Weather Underground, 2009. Detailed history and climate. WunderMap new. web page

Wen, X. and X. Yang, 2008. An operational improvement of haze/clear line identification from satellite imagery based on multi-resolution segmentation. Proceedings of the 2nd International Symposium on Intelligent Information Technology Application, Dec. 20-22, Shanghai, pp: 571-575.

Williams, D., 2009. Landsat 7 Science Data Users Handbook. Elsevier, USA.

Xingna, Y.U., Z.H.U. Bin, F.A.N. Shuxian, Y.I.N. Yan and B.U. Xiaoli, 2009. Ground-based observation of aerosol optical properties in Lanzhou, China. J. Environ. Sci., 21: 1519-1524.